

Article

Modeling of Lithium Plating and Stripping Dynamics during Fast Charging

Polina Brodsky Ringler ^{1,†}, Matthew Wise ^{2,†}, Prashanth Ramesh ^{3,†}, Jung Hyun Kim ^{3,†}, Marcello Canova ^{3,*†}, Chulheung Bae ^{4,†}, Jie Deng ^{4,†}  and Heechan Park ⁵

¹ Department of Mechanical Engineering, Colorado School of Mines, Golden, CO 80401, USA; pbringler@mines.edu

² Schaeffler Group USA, Wooster, OH 44691, USA; wisemtt@schaefller.com

³ Center for Automotive Research, The Ohio State University, Columbus, OH 43210, USA; ramesh.47@osu.edu (P.R.); kim.6776@osu.edu (J.H.K.)

⁴ Ford Motor Company, Dearborn, MI 48126, USA; cbae@ford.com (C.B.); jdeng9@ford.com (J.D.)

⁵ SK On, Daejeon 34124, Republic of Korea; parkhc@sk.com

* Correspondence: canova.1@osu.edu; Tel.: +1-614-247-2336

† These authors contributed equally to this work.

Abstract: This paper proposes a new model that predicts the cell voltage dynamics and capacity degradation induced by lithium plating and stripping. The proposed model uses a single equilibrium reaction to describe the deposition and dissolution of metallic lithium, predicting the partial reversibility of the plating/stripping reaction, the characteristic voltage plateau during relaxation, and the capacity loss due to the Loss of Cyclable Lithium (LCL). The model is integrated with a Doyle–Fuller–Newman (DFN) electrochemical model, calibrated and validated with experimental data. The model has the potential to improve the accuracy of predicting the effects of lithium plating in Li-ion cells and aid in the development of Extreme Fast Charging (XFC) technology for BEVs.

Keywords: fast charging; lithium plating; modeling



Citation: Brodsky Ringler, P.; Wise, M.; Ramesh, P.; Kim, J.H.; Canova, M.; Bae, C.; Deng, J.; Park, H. Modeling of Lithium Plating and Stripping Dynamics during Fast Charging. *Batteries* **2023**, *9*, 337. <https://doi.org/10.3390/batteries9070337>

Academic Editors: Matthieu Dubarry, Junnan Hao and Pascal Venet

Received: 14 April 2023

Revised: 25 May 2023

Accepted: 15 June 2023

Published: 21 June 2023



Copyright: © 2023 by the authors. Licensee MDPI, Basel, Switzerland. This article is an open access article distributed under the terms and conditions of the Creative Commons Attribution (CC BY) license (<https://creativecommons.org/licenses/by/4.0/>).

1. Introduction

Enabling Extreme Fast Charging (XFC) is a key priority for increasing the adoption of Battery Electric Vehicles (BEVs) and decarbonizing the transportation sector. On the other hand, lithium ion (Li-ion) cell technology is currently limited in terms of charge rate capability by a side reaction known as lithium plating, in which solid metallic lithium forms in the anode, where its local potential falls below the potential of solid lithium [1]. Lithium plating has been shown to be favored at low temperatures, high State of Charge (SOC) and high rates of charging, which leads to lower intercalation rates, larger overpotentials, values of the anode Open Circuit Potential (OCP) close to 0V (vs. Li/Li^+), and slower solid-phase diffusion [2–5]. While the plating reaction can be partially reversible, irreversibly plated lithium can form solid dendrites, leading to a loss in the accessible surface area of the anode active material and a loss of cyclable lithium through formation of a Solid Electrolyte Interface (SEI) [6–9].

Due to the practical challenges of measuring the onset of plating in a commercial cell in situ during fast charging, modeling and simulation resources have received considerable attention [10–12]. Methods to predict the lithium plating and its effects on capacity loss have been created by postulating different mechanisms, rates, and locations of these phenomena [1,13–18]. On the other hand, capturing the interactions between the side reactions and the lithium intercalation in the anode during the cell charging and subsequent relaxation is rather complex due to the dynamics and couplings inherent to this process. A lack of fidelity in modeling these effects ultimately limits the ability of models to predict the characteristic voltage response that can be observed from experimental tests when plating occurs.

This paper proposes a new model that predicts the cell voltage dynamics and capacity degradation induced by lithium plating and stripping via a single side reaction. Most plating models assume that the plating and stripping reaction kinetics are described by two separate equations. However, this assumption contrasts with the principles of equilibrium reactions, in that a cathodic and an anodic reaction are simultaneously present at the same electrode/electrolyte interface. According to this assumption, the lithium plating and stripping kinetics can be described using a single equation. In this study, a single equilibrium reaction is used to describe the deposition and dissolution of metallic lithium. The resulting model predicts the partial reversibility of the plating/stripping reaction, the characteristic voltage plateau during relaxation, and the capacity loss due to the Loss of Cyclable Lithium (LCL). The model is validated with experimental data to show the ability to correctly represent the process.

The paper is organized as follows: Section 2 presents the experimental tests and data analysis for lithium plating detection and capacity loss analysis. Section 3 illustrates the plating/stripping model. Section 4 describes the integration of the model with a Doyle–Fuller–Newman (DFN) electrochemical model, the calibration process, and verification.

2. Experimental Tests and Results

A small format, 1.6 Ah pouch cell with commercial-grade electrodes was selected for the experimental study. The 50×50 mm cell contains a blended NMC811 and NMC111 cathode and a blended artificial and natural graphite anode and utilizes a 1M LiPF₆ electrolyte with a ceramic coated separator.

The pouch cells were retrofitted by inserting a reference electrode, providing an in-situ, non-destructive method to measure anode potential. After conducting initial tests for baseline capacity and internal resistance, the cells were pierced in one of the lower corners, and a 22 AWG copper wire was inserted into the cell. Prior to the insertion, the copper wire was coated in solid lithium using electroplating to ensure proper electrical contact and minimize noise in the measurements. After the insertion, electrolyte solvent was injected into the cell, and the hole was sealed with an epoxy resin [19]. Figure 1 shows a schematic of the reference electrode insertion.

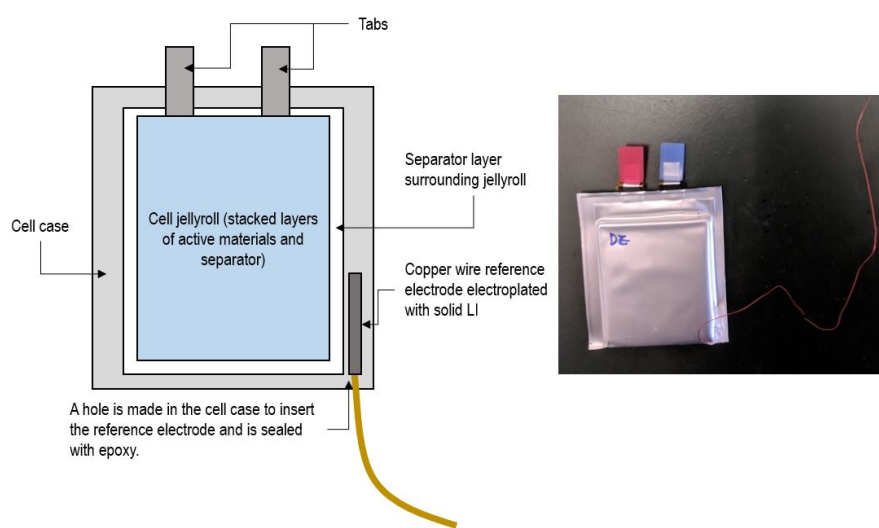


Figure 1. Li-ion pouch cell setup with lateral reference electrode.

The retrofitted cells were then placed in an aluminum fixture to apply pressure (34 kPa) and temperature control via Peltier junctions. The cells were cycled with a 0–5 V Arbin Instruments LBT21044 eight-channel battery cycler, capable of a current range of 0–100/10/1/0.1 A with 100 ppm precision.

After a baseline characterization, a series of fast charge tests was performed at three different temperatures ($0\text{ }^{\circ}\text{C}$, $10\text{ }^{\circ}\text{C}$, $25\text{ }^{\circ}\text{C}$). In this protocol, a cell is charged starting from a low SOC at a constant current (CC) until the terminal voltage of the cell reaches the maximum cell voltage cutoff (4.2V), and then the charge mode is switched to constant voltage (CV). As discussed in [18,20–27], one of the most accessible detection methods in-situ for the presence of Li-plating in a charge cycle consists of a plateau in cell voltage during relaxation. Figure 2 shows the difference in terminal voltage during cell relaxation between typical settling behavior and a voltage plateau indicative of the Li-stripping side reaction, which indirectly indicates that Li-plating has occurred during the preceding cell charging.

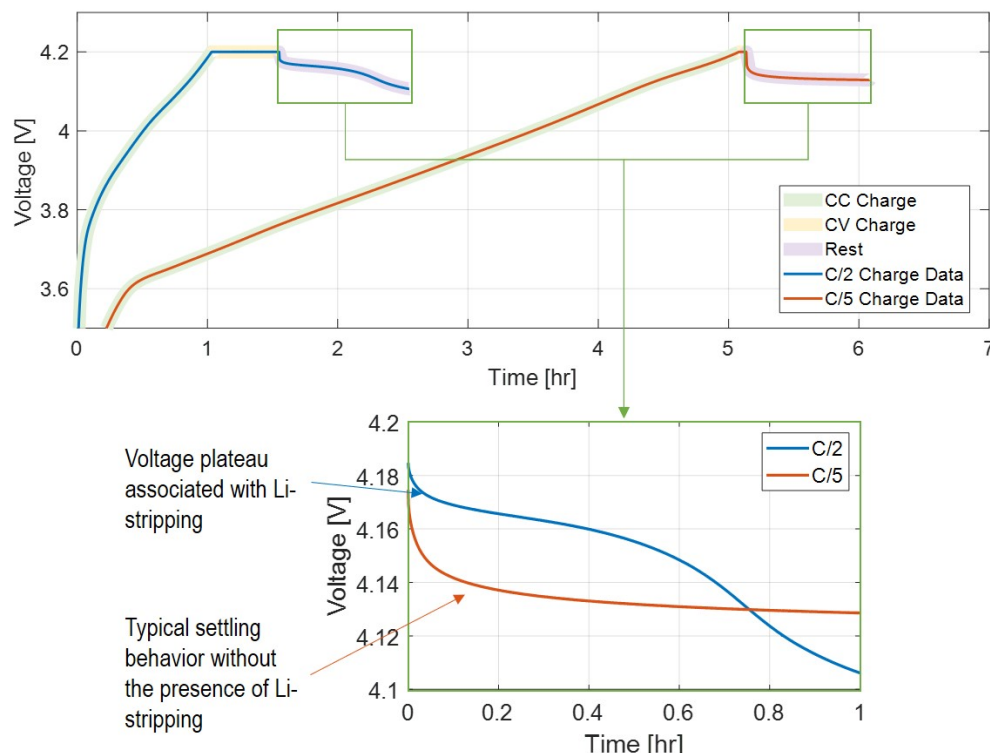


Figure 2. Experiment cell terminal voltage during relaxation for a typical charge cycle vs. a cycle indicating the presence of Li-stripping.

According to literature, plating can occur when the local anode potential falls below 0 V vs. Li/Li^{+} [1,18,23,26,28,29]. If charging ends while Li-plating is still occurring, or if the overpotential is sufficiently small to cause the anode potential to rise above 0 V vs. Li/Li^{+} , the plating reaction will reverse (stripping), leading to a characteristic plateau in the voltage [15,18,21,23,26,30,31].

It is noteworthy to observe that plating may extend through the early phase of the CV portion during a CC-CV charging event. If charging ends while lithium is still plating, the stripping reaction will begin as soon as the anode potential rises above 0 V . This appears as a voltage plateau as the cell relaxes, as shown experimentally in Figure 3. This figure (relative to a 5C charge with a 1C CV cutoff at $25\text{ }^{\circ}\text{C}$) indicates the occurrence of Li-stripping by the presence of a peak in the rate change of the cell voltage profile (dV/dt) during relaxation, which is equivalent to the characteristic voltage plateau.

On the other hand, if the anode potential rises above 0 V vs Li/Li^{+} during the CV phase, the stripping process will begin while the cell is still charged. Because the voltage is held constant, the transition to stripping during the CV phase can be detected by monitoring the rate of change in current (dI/dt), which displays a characteristic peak when the stripping side reaction begins. Figure 4 illustrates this behavior for a CC-CV charge at 4.2 V with a C/10 CV cutoff at $25\text{ }^{\circ}\text{C}$.

It should be noted that while the plateau in the voltage profile during relaxation is commonly assessed in the literature as an indicator of Li-stripping [22,28,32–34], the peak in the applied current during the CV phase under very low currents is a novel indicator of stripping in this study. The presence of a plating-to-stripping transition during CV charging is strongly dependent on the parameters of the CC–CV charge profiles. For the cells tested in this study, the transition occurred during the CV phase, when the target cell voltage was 4.2 V and the cutoff current was set lower than C/2 at 25 °C.

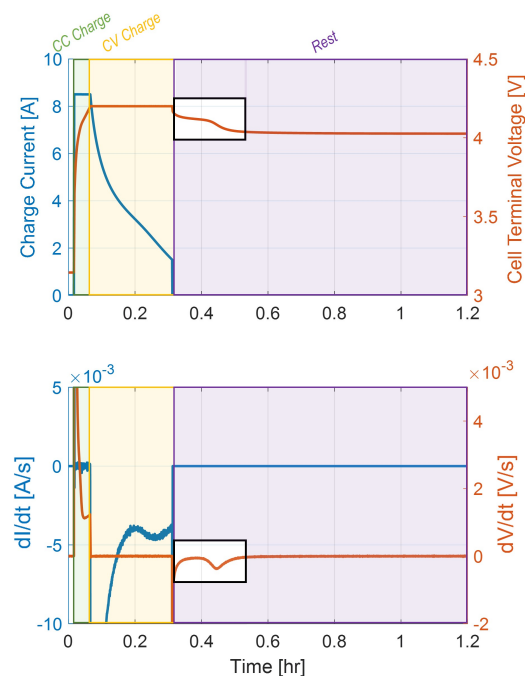


Figure 3. Example of lithium stripping detection for CC–CV charging profile during rest.

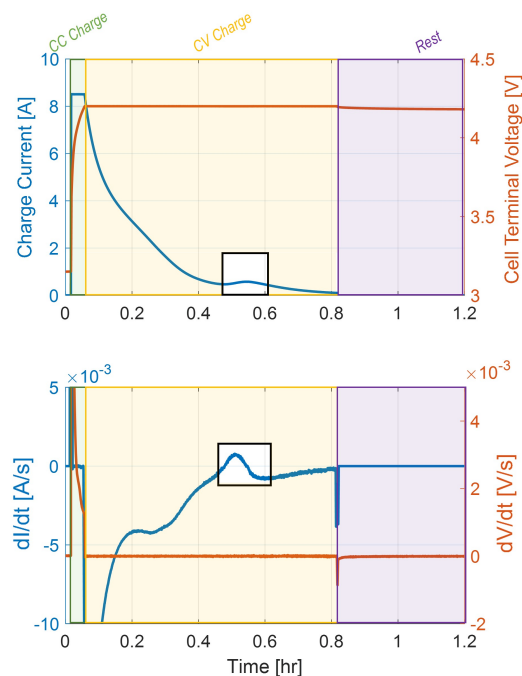


Figure 4. Example of lithium stripping detection for CC–CV charging profile during CV phase.

The magnitude of the CC current and the CV cutoff voltage were varied to explore their effects on the onset of Li-plating in the cell. For each selected CC charge rate and CV current cutoff, the cell was charged to its maximum cutoff voltage, charged at CV until the set cutoff current, allowed to rest for 4 h, and then discharged at C/5 to its minimum cutoff voltage to perform a capacity test.

For each tested condition, the rate change of the voltage profile was analyzed for the indicative peak in the dV/dt profile. If a peak is present, this suggests that a voltage plateau has occurred during the relaxation after the charge, which indicates the presence of Li-stripping and, by consequence, of Li-plating. The current profile during the CV phase was also analyzed to detect a localized increase in the current decay profile (or the peak in the dI/dt profile), which may be indicative of an Li-stripping side reaction occurring during CV charge. If no voltage plateau was present in the relaxation voltage data or peaks present in the CV current profile, it was determined that there was no indicative sign of Li-stripping in the reaction. This investigation was repeated for multiple C-rates and cutoff currents for CV, and the presence of an Li-stripping plateau in each test is tabulated in Table 1 for tests performed at 25 °C.

Table 1. Li-plating test conditions and results of Li-stripping plateau detection.

CC Charge Rate	CV Current Cutoff		
	None (CC Only)	1.5 A	0.1 A
4C	Stripping during relaxation	Stripping during relaxation	Stripping during CV
5C	Stripping during relaxation	Stripping during relaxation	Stripping during CV
6C	No Stripping	Stripping during relaxation	Stripping during CV

A summary of the outcomes of all tests performed at the three chosen temperatures is shown in Figure 5. Here, it can be seen that varying the C-rate for CC charging, the CV cutoff current, and the cell temperature changes the lithium stripping behavior in the cell, and that this behavior is sensitive to the charge conditions which include temperature, charge current, and CV current cutoff.

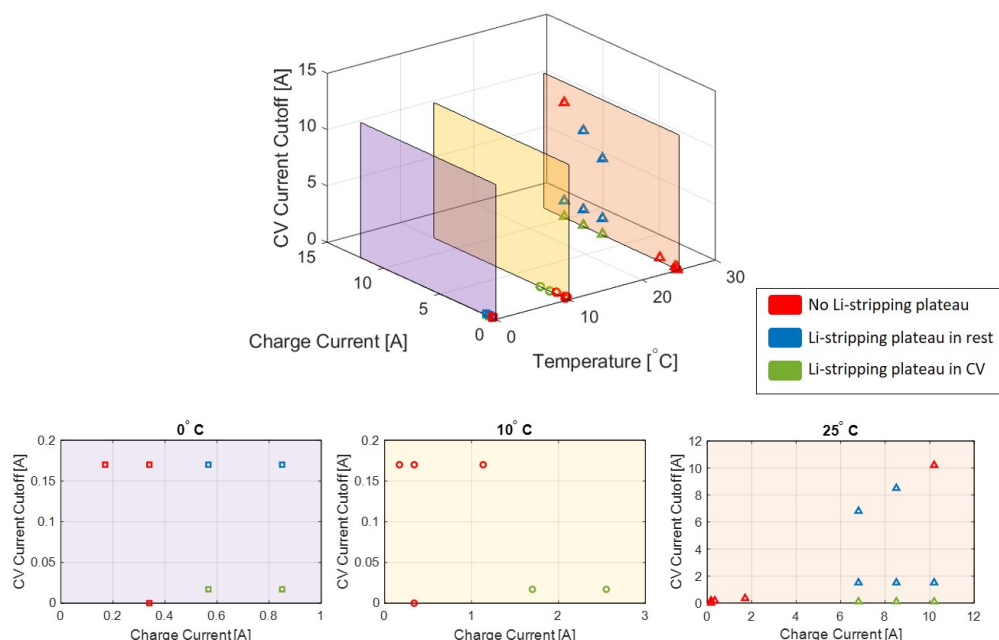


Figure 5. Summary of all experimental charge results and occurrence of stripping plateau.

As documented in the literature and verified in these experiments, Li-plating increases with increased charge current and decreased temperature. At 0 °C, there were signs of Li-stripping (and thus Li-plating) at charge rates as low as C/3, while Li-plating did not occur in the same charge cycles at 10 °C until rates of 1C and at 25 °C until rates of 3C.

The CV cutoff, which has an impact when the Li-stripping plateau occurs (during CV or during relaxation), can provide additional insight into the behavior of the anode during the plating/stripping portion of the charge cycle. Figure 6 highlights how studying the effects of the CV cutoff at one fixed CC charge rate can give insight into the behavior of the anode potential in situ.

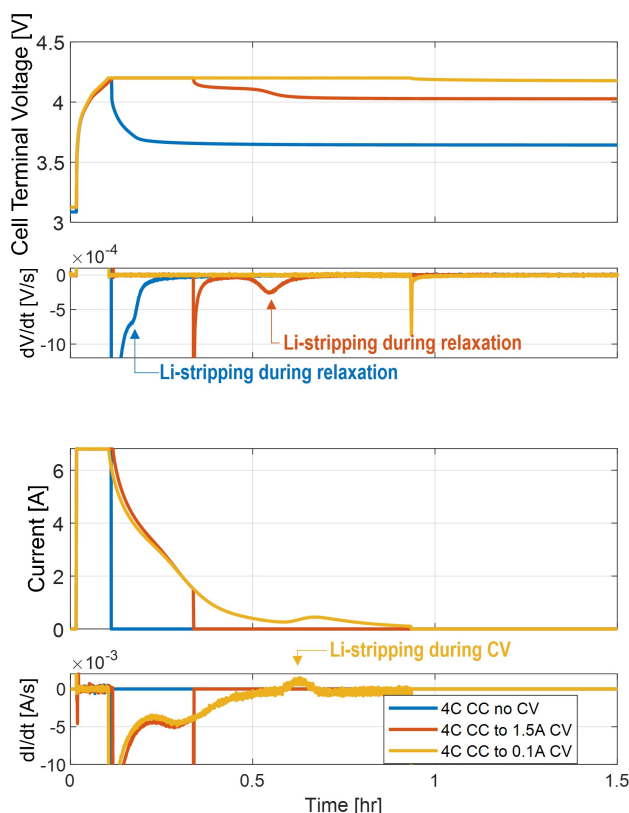


Figure 6. Example of various 4C charge profiles at 25 °C with various CV cutoffs and implications on plating.

In the 4C charge test with no CV portion (CC only), there is a very small plateau associated with the occurrence of Li-stripping during the rest phase. In the 4C charge with a 1.5 A CV cutoff current, there is a more noticeable and distinct voltage plateau, which lasts longer after charge is cut off in the cell. When the cell is charged at 4C with a 0.1 A CV cutoff current, Li-stripping occurs during the CV phase.

From these conditions, it can be deduced that in all three charge conditions, the anode reaches a potential of less than 0 V vs Li/Li^+ during the CC charge portion. In fact, even with the 4C charge with no CV, there are signs of Li-stripping, indicating that Li-plating has occurred. The 4C charge with a 1.5A CV cutoff current exhibits a longer and more distinct voltage plateau, indicating that more Li-stripping is occurring after this charge and implying that this is caused by more Li-plating. Because the voltage plateau happens after charge is stopped, the anode must be plating (at < 0V vs. Li/Li^+) during the entire CV mode in this charge cycle. This indicates that the Li-plating starts in the CC region (as seen in the 4C charge with no CV) and continues through the CV region until the 1.5 A charge current cutoff. In the longer CV test (at which the CV current is cut off at 0.1 A), the plateau occurs around the point at which the cell is being charged at 0.5 A. Because the current peak

indicates the occurrence of an Li-stripping side reaction, this represents the point at which the anode potential rises above 0 V to transition from the Li-plating to Li-stripping reaction.

These sequential charges at different rates, exemplified in Figure 6, can shed further light on the anode behavior during different portions of the charge phase and can lend understanding to both the onset and stop of the Li-plating and allow the charge region to be broken into the regions shown in Figure 7.

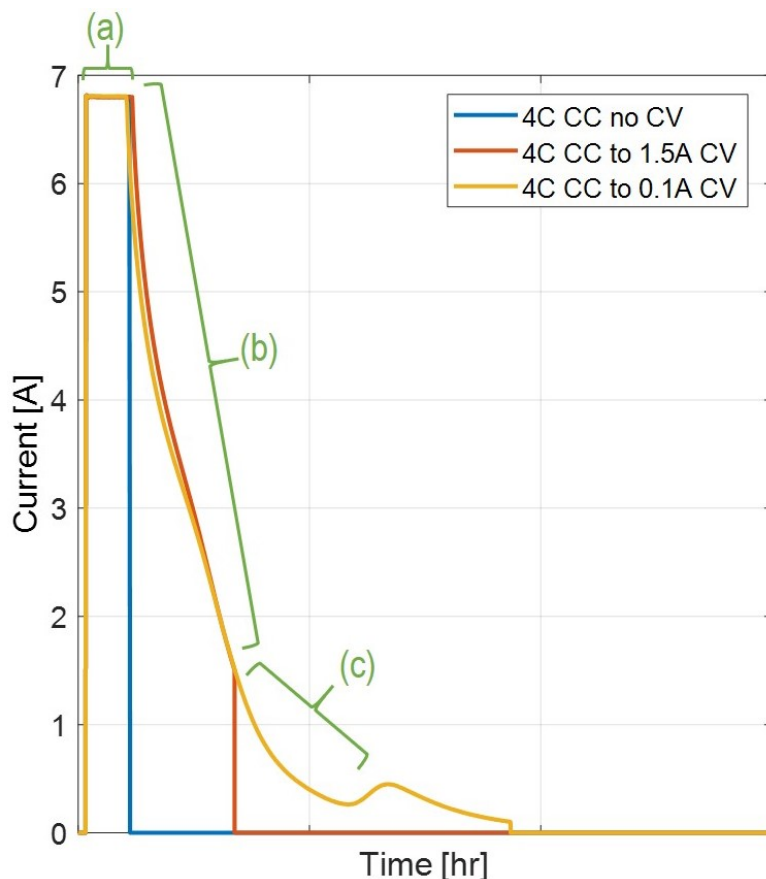


Figure 7. Understanding of charge regions from 4C charge profiles at 25 °C with various CV cutoffs and implications on plating.

In region (a), the anode reaches the Li-plating favored potential lower than 0 V vs Li/Li^+ and maintains this condition through region (b). Region (c) indicates the final portions of the Li-plating condition being favored before the cell transitions into conditions of Li-stripping, when the anode rises to a potential greater than 0 V vs Li/Li^+ . This methodology of mapping various charge profiles to indicators of anode behavior can help to give insight into the underlying mechanisms and conditions favoring Li-plating. Additionally, this provides a useful data set for the model calibration explored in this work.

3. Modeling

The lithium plating side reaction is a local phenomenon that can occur in parallel with the intercalation and other degradation mechanisms. As pointed out in the literature—see for instance [28]—plating often occurs in conjunction with other side reactions, such as SEI layer growth. On the other hand, for a low number of consecutive charge cycles at high C-rate conditions, as performed in the experiments described in this paper, it is reasonable to assume that the amount of capacity loss due to SEI layer growth is minimal compared to plating. This allows us to simplify the integration of the plating/stripping model into an electrochemical model.

If the local potential of the anode drops below the potential of solid Li (<0V vs. Li/Li^+), the lithium plating side reaction is favored [1,18,23,28]. The process of deposition and dissolution of the solid lithium can be implemented as a side reaction occurring at each location within the anode thickness. The reference reaction can be written as



The deposition and dissolution of metallic lithium is described by a single Butler–Volmer equation:

$$j_{Li} = i_{0,Li} \left[\frac{c_{Li}}{c_{Li}^{eq}} \exp\left(\frac{\alpha_{a,Li} F}{RT} \eta_{Li}\right) - \frac{c_e}{c_e^{eq}} \exp\left(\frac{-\alpha_{c,Li} F}{RT} \eta_{Li}\right) \right] \quad (2)$$

where j_{Li} is the side reaction current density, $i_{0,Li}$ is the exchange current density, $\alpha_{a,Li}$ and $\alpha_{c,Li}$ are the respective anodic and cathodic transfer coefficients for the plating/stripping reaction, c_{Li} is the concentration of Li metal, c_e is the concentration of Li^+ in the electrolyte, c_{Li}^{eq} and c_e^{eq} are the bulk concentrations of Li metal and ions in the electrolyte respectively, R is the universal gas constant, T is the temperature, and F is Faraday's constant.

The lithium overpotential η_{Li} is defined as

$$\eta_{Li} = \phi_s - \phi_e - U_{Li} \quad (3)$$

where ϕ_s is the local solid phase potential, ϕ_e is the local electrolyte potential, and U_{Li} is the equilibrium potential of metallic lithium.

The exchange current density for the side reaction is calculated by

$$i_{0,Li} = F k_{0,Li} (c_{Li}^{eq})^{\alpha_{c,Li}} (c_e^{eq})^{\alpha_{a,Li}} \quad (4)$$

where $k_{0,Li}$ is the reaction rate constant of the plating/stripping reaction. Since the deposition/dissolution reaction is modeled as homogeneous along the surface, the lithium concentration is set to 1 when plated lithium is present, causing the amount of plated lithium to not affect the reaction rate. When plated lithium is not present, the concentration is set to 0 so that stripping does not occur. A correction term $\left(\frac{\beta n_{Li,rev}}{1+\beta n_{Li,rev}}\right)$ on the anodic branch replaces this plated lithium concentration to bulk concentration ratio $(\frac{c_{Li}}{c_{Li}^{eq}})$ to compute the stripping side reaction within the Butler–Volmer equation [28].

$$j_{Li} = i_{0,Li} \left[\left(\frac{\beta n_{Li,rev}}{1 + \beta n_{Li,rev}} \right) \exp\left(\frac{\alpha_{a,Li} F}{RT} \eta_{Li}\right) - \frac{c_e}{c_e^{eq}} \exp\left(\frac{-\alpha_{c,Li} F}{RT} \eta_{Li}\right) \right] \quad (5)$$

where $n_{Li,rev}$ is the quantity of reversibly plated lithium, and β is a large value to effectively make the $\left(\frac{\beta n_{Li,rev}}{1 + \beta n_{Li,rev}}\right)$ term equal 1 when $n_{Li,rev} \gg 1$, and 0 when $n_{Li,rev} = 0$. The inclusion of this term in Equation (5) allows us to compute the current density for the stripping reaction while reversibly plated lithium is present and restricts stripping when the reversibly plated lithium is not present.

At each node, the amount of plated lithium is calculated by integrating the side reaction current:

$$\frac{dn_{Li}}{dt} = -\frac{a_n}{F} \cdot j_{Li} \quad (6)$$

where n_{Li} is the quantity of plated lithium, and a_n is the surface area of the anode. It is assumed that a portion of the plated lithium becomes electrically inactive and no longer participates in the reaction. The reversibility of the plating reaction is governed by

$$\frac{dn_{Li,rev}}{dt} = -\eta_r \frac{a_n}{F} \cdot j_{Li} \quad (7)$$

$$\frac{dn_{Li,irr}}{dt} = -(1 - \eta_r) \frac{a_n}{F} \cdot j_{Li} \quad (8)$$

which introduces a “reversibility factor” η_r as a function of current sign:

$$\eta_r = \alpha + 0.5(1 - \alpha) \left(1 + \frac{\arctan(kj_{Li})}{90} \right) \quad (9)$$

where α is the reversible fraction of plated lithium (tunable parameter), and k is a large number.

During plating ($j_{Li} < 0$), the side reaction current leads to the accumulation of both irreversible and reversible plated lithium. When stripping is favored ($j_{Li} \geq 0$), the side reaction current contributes to removing only the reversibly plated lithium. The total quantity of plated lithium at each location within the anode thickness is the sum of the reversible and irreversible parts:

$$n_{Li,tot}(x, t) = n_{Li,irr}(x, t) + n_{Li,rev}(x, t) \quad (10)$$

4. Integration with P2D Model

The plating and stripping model can be integrated into any electrochemical Li-ion cell model as a side reaction. In this work, the Doyle–Fuller–Newman (or Pseudo Two Dimensional, P2D) model was utilized as the source model due to its ability to predict the distribution of lithium concentration and potential through the thickness of the electrodes [35,36].

The P2D model assumes uniform use of the electrodes in the planar direction (i.e., uniform intercalation across anode surface). For this reason, this work assumes the same uniform Li plating/stripping on the anode surface.

The side reaction current density j_{Li} represents both the forward lithium plating and reverse Li-stripping reactions. The lithium plating side reaction occurs in parallel with the intercalation/deintercalation of graphite. At each location within the anode, the net current density (j_n) is split between the side reaction current density (j_{Li}) and the intercalation/deintercalation current density (j_{int}):

$$j_n(x, t) = j_{Li}(x, t) + j_{int}(x, t) \quad (11)$$

Figure 8 illustrates the concept. When any location in the anode reaches a potential favoring the plating side reaction, the amount of plated lithium n_{Li} grows due to Equation (6). This process occurs in parallel with the intercalation reaction, described by j_{int} . This net current density is the same magnitude of the current density that is subtracted from the electrolyte solution at each location through the electrode thickness.

When the local potential no longer favors the Li-plating side reaction and there is reversible plated lithium present on the particle ($n_{Li,rev} \geq 0$), the amount of plated lithium decreases as described by Equations (5) and (7). The side reaction current density that dissolves the reversible lithium results in an increased local concentration of ionic lithium in the electrolyte solution, with successive intercalation into the graphite.

Since the magnitude of the plating reaction is dependent on the local value of the anode potential in both location and time, there can be different amounts of plated lithium at different locations within the anode domain as the cell is charged.

The model was integrated within PyBaMM, an open-source Python implementation of the P2D model [36]. Figure 9 illustrates the essential equations of the P2D model and its interaction with the plating and stripping model, via block diagram representation.

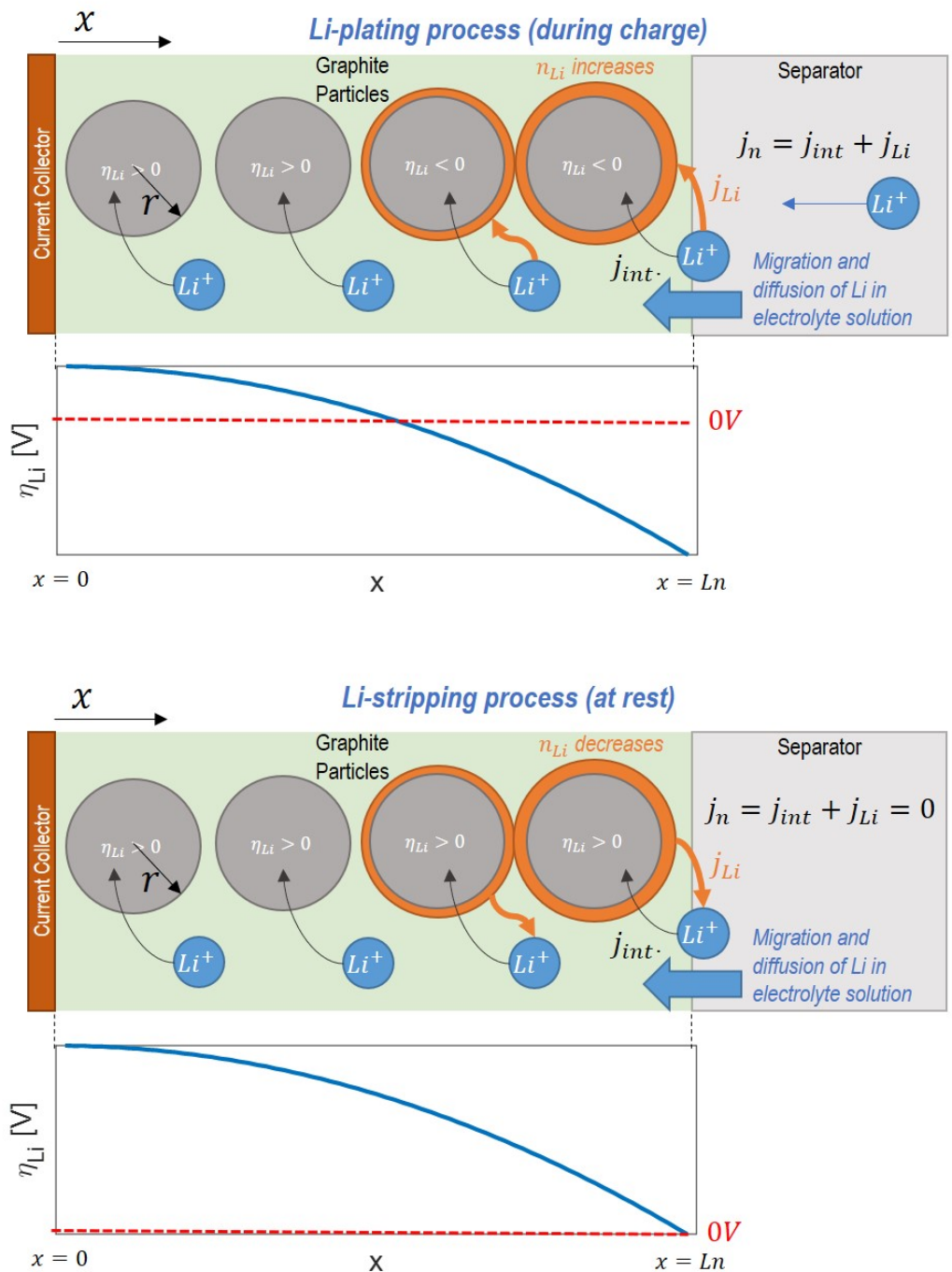


Figure 8. Mechanism of plating and stripping reactions integrated in P2D model.

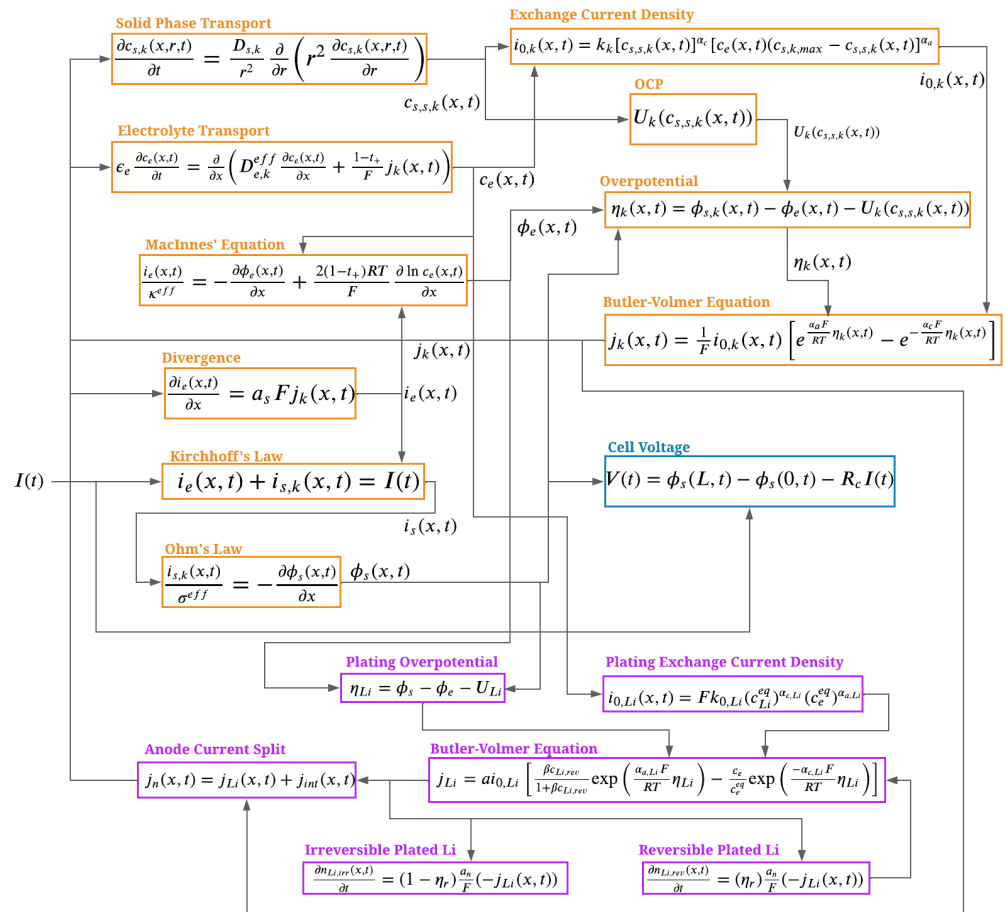


Figure 9. Block Diagram of P2D Model with Integrated Plating/Stripping Model.

5. Calibration and Verification

The plating and stripping model has two parameters for calibration, namely the reaction rate constant $k_{0,Li}$ and the degree of reversibility α . The reaction rate parameter affects the exchange current density for the plating and stripping reaction and is the main fitting parameter. The model behaviors for different $k_{0,Li}$ values are presented in Figure 10.

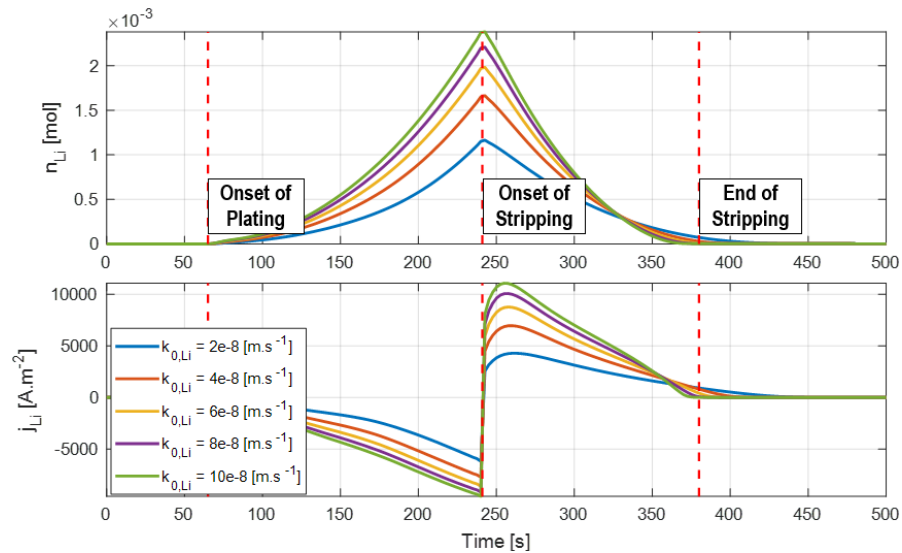


Figure 10. Plating/stripping behavior for different values of $k_{0,Li}$ (5C CC fast charge).

While the parameter $k_{0,Li}$ dictates the amount of lithium plating that occurs, the duration of the plating/stripping process is mainly dependent on the overpotential η_{Li} . For this reason, accurate prediction of the anode potential (which requires use of reference electrode data) during fast charging is critical to correctly capture the intercalation and plating reactions.

The voltage plateau associated with the stripping reaction during cell relaxation is commonly used to calibrate the reaction rate constant. When stripping induces a voltage plateau, the magnitude of the peak in the differential voltage is an indication of the quantity of lithium being stripped away, so the reaction rate constant can be tuned to match this peak. Figure 11 shows how the voltage and differential voltage profiles during relaxation are affected by changes in the reaction rates for the formation/dissolution of metallic lithium.

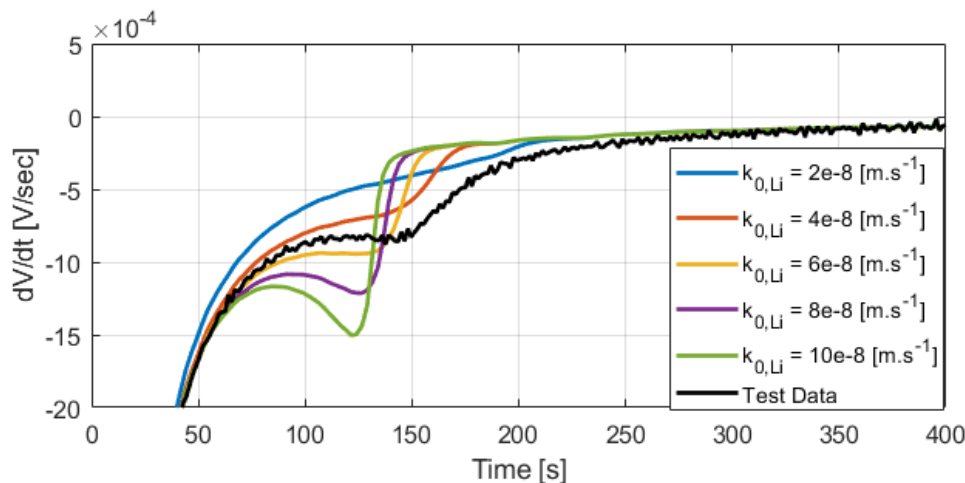


Figure 11. Effects of $k_{0,Li}$ parameter on voltage derivative during relaxation (5C CC fast charge).

One single fast charging test (5C CC fast charge) was used to calibrate the parameter $k_{0,Li}$. The differential voltage profiles in Figure 12 and 13 show good agreement between the model and the data for other test conditions.

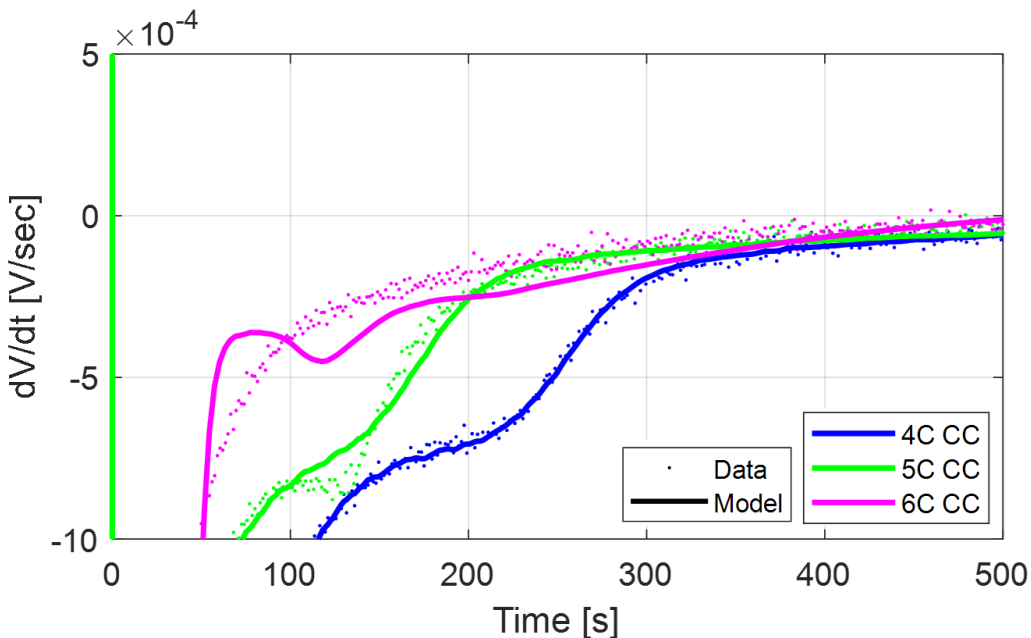


Figure 12. Verification of calibrated $k_{0,Li}$ parameter for CC fast charge tests.

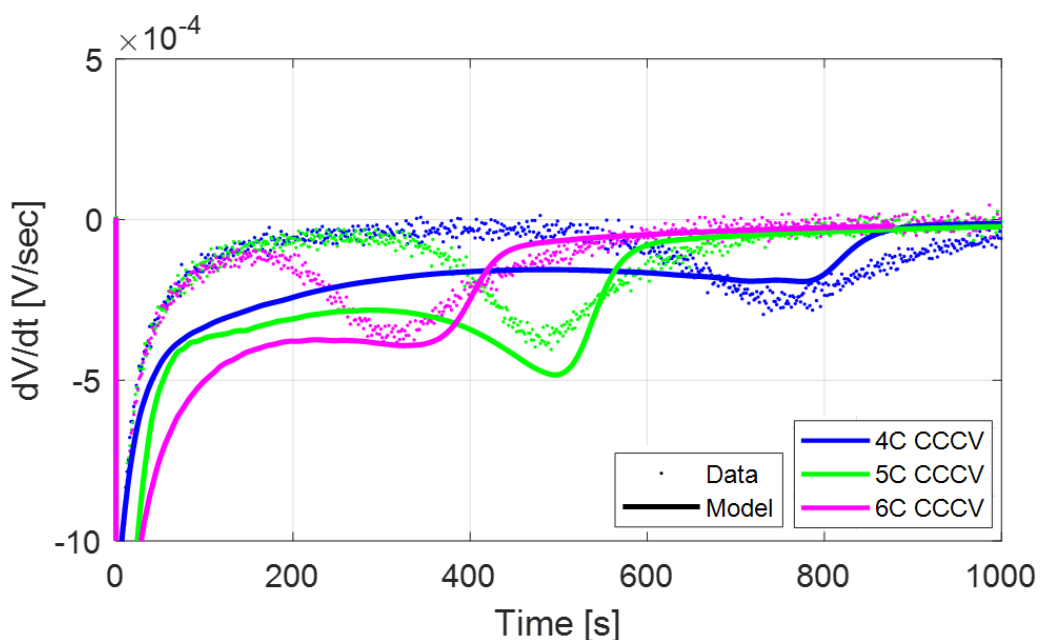


Figure 13. Verification of calibrated $k_{0,Li}$ parameter for CC–CV fast charge tests.

In Figure 12, the modeled 4C CC relaxation dV/dt has an early peak occurring at 90 s that is not observed in the data. This peak is caused by a characteristic cathode OCP slope change and is not related to the lithium stripping side reaction.

In Figure 13, the model presents errors in capturing the relaxation dV/dt curves at 4C and 6C for the CC-CV test. The errors might be the result of an imperfect model calibration at Beginning of Life (BOL), rather than issues with the stripping model. In fact, although the predicted dV/dt profile does not exactly match the data, the time of occurrence of the stripping peak matches quite well, which indirectly proves that the model is correctly predicting the onset of the stripping behavior.

The reversibility parameter α governs the fraction of reversible and irreversible plated lithium and can be calibrated to match capacity test data following a fast charging cycle. To this extent, the C/20 discharge test data were used to compute the capacity reduction after each fast charge cycle. Since severe capacity fade is observed within just a few charge cycles, it can be assumed that the main aging mechanism causing this degradation is lithium plating.

Simulations of consecutive fast charge cycles (4C, 5C, then 6C) were conducted to predict the quantity of irreversibly plated lithium, from which the capacity loss was computed via Faraday's law:

$$Q_{pl} = \frac{n_{Li}F}{3600} \quad (12)$$

The reversibility parameter α was tuned to match the capacity fade experienced due to CC fast charging (Figure 14).

Note that changing the reversibility of the side reaction impacts the accuracy of the voltage plateau prediction, requiring further tuning after capacity loss data are matched. The final calibrated lithium plating parameters are provided in Table 2. As previously mentioned, once the reaction rate parameter $k_{0,Li}$ is tuned to match the relaxation profile, the reversibility parameter α can be calibrated to match the capacity loss, which is measured in the C/20 discharge experiments. Figure 14 shows how the model can match the capacity loss from lithium plating by calibrating the α parameter.

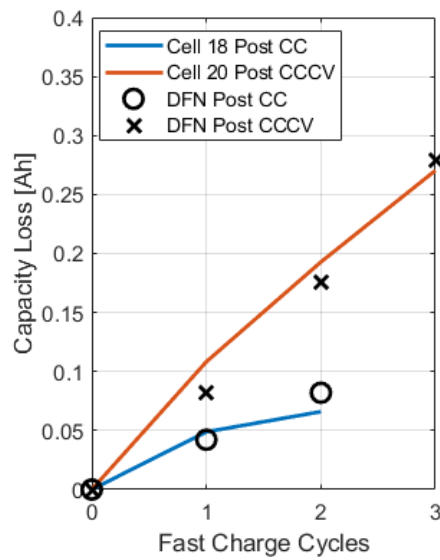


Figure 14. Modeled capacity agreement with RPT measured capacity loss.

Table 2. Calibrated plating model parameters.

Plating Parameters	Value
Rate Constant $k_{0,Li}$	$5.5 \times 10^{-8} [\text{m/s}]$
Reversibility α	0.65 [-]

6. Simulation and Analysis

The model predictions can be further analyzed to understand the behavior of the cell during Li-plating and Li-stripping conditions. Figure 15 illustrates the phenomenon of Li-stripping during relaxation, namely how the profile of plated lithium through the anode thickness changes as it is oxidized and returns to the electrolyte solution during the rest period.

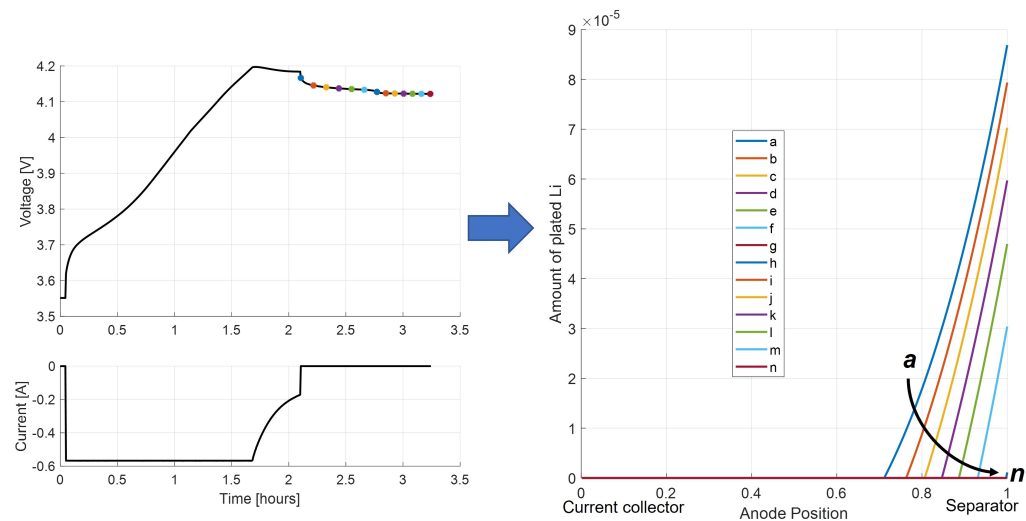


Figure 15. Investigation of plated lithium quantity through the anode thickness after relaxation with the DFN model.

The individual points in the Li-stripping plateau in time show that the amount of plated lithium decreases at each time step, with the peak of plated lithium located at the

interface with the separator. As the stripping process continues, each location in the cell where plated lithium exists becomes progressively depleted.

Investigation of the net anodic current density ($j_n = j_{int} + j_{Li}$) in Figure 16 during Li-stripping shows a location-dependent net current. At the interface between the anode and separator, the net anodic current is positive, meaning the oxidation reaction is favored. This means that there is a positive contribution of lithium from the stripping reaction, since there is a larger quantity of accumulated lithium in these regions as confirmed in Figure 15. Closer to the current collector, the net anodic current density is negative, meaning that the reduction reaction is favored. Here, the net reaction is the charge of the graphite from stripped Li intercalating back into the anode. Because lithium stripping is favored near the separator side of the anode but lithium intercalation is favored on the current collector side, this implies the net movement of lithium ions from the separator to current collector side of the anode as the stripping reaction occurs.

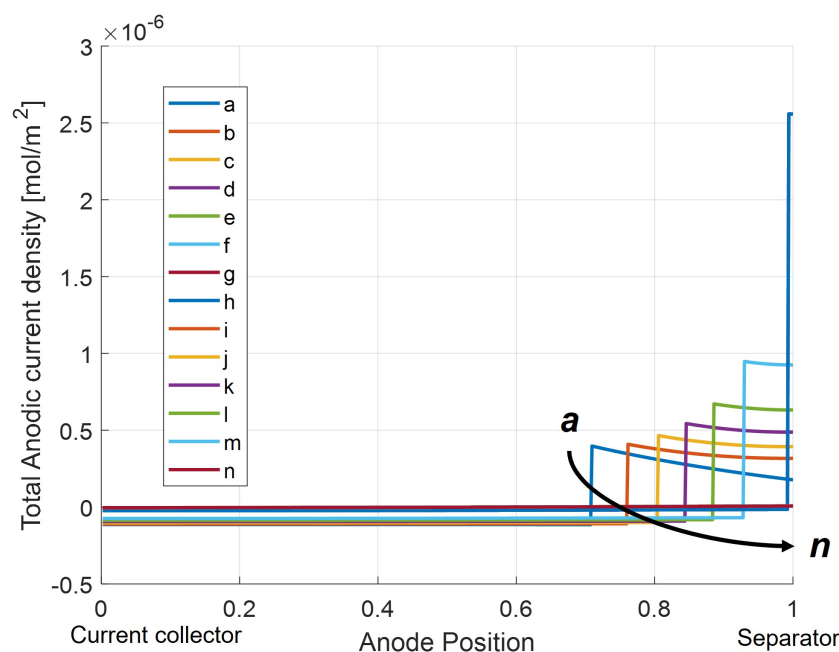
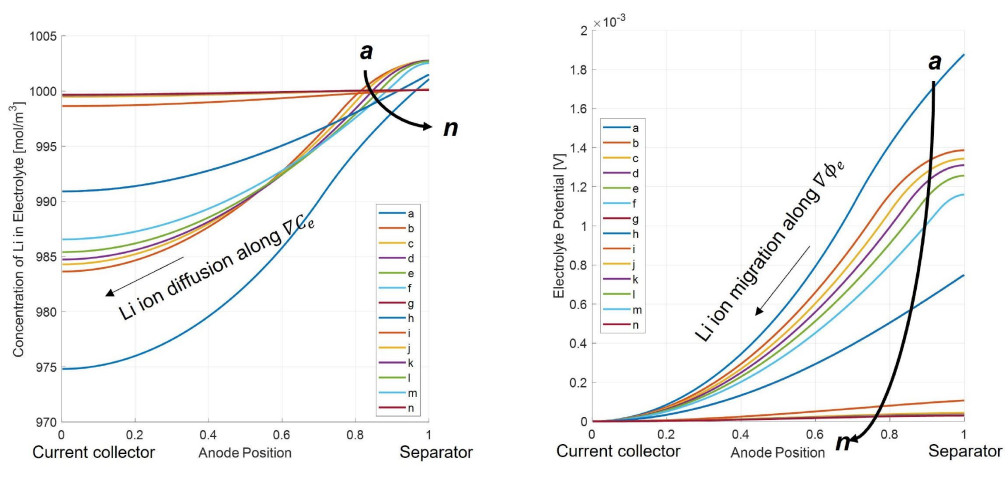


Figure 16. Investigation of anodic current density through the anode thickness after relaxation with the DFN model.

Figure 17 confirms that as lithium strips from the surface of the graphite particles, it moves towards the current collector side of the anode to re-intercalate back into the graphite material. As the concentration of lithium in the electrolyte increases, ionic diffusion drives the movement of lithium towards the current collector, where less lithium is in solution due to the lack of stripping in this region of the anode. Additionally, the potential gradient in the electrolyte solution after charge favors the migration of Lithium towards the current collector, as there is a higher potential in the liquid phase on the separator side of the anode.



(a) Concentration gradient in electrolyte solution.
(b) Potential gradient in electrolyte solution

Figure 17. Concentration and potential gradients in the electrolyte solution.

7. Conclusions

This paper proposes a new model that predicts the cell voltage dynamics and capacity degradation induced by lithium plating and stripping. Unlike most models that utilize multiple reactions to describe the process, a single equilibrium reaction is here derived to describe the deposition and dissolution of metallic lithium. The resulting model predicts the partial reversibility of the plating/stripping reaction, the characteristic voltage plateau during relaxation, and the capacity loss due to the Loss of Cyclable Lithium (LCL).

The plating and stripping model was integrated with a Doyle–Fuller–Newman (DFN) electrochemical model, calibrated and validated with experimental data to show the ability to correctly represent the process. The model described in this paper can be utilized to analyze the physical phenomena occurring in the cell during fast charging, giving better insight into the cell's behavior during this undesirable side reaction. If the behavior can be better predicted and understood and the root causes and dynamics of the Li-plating and Li-stripping reactions can be quantified, these models can be used for design studies for cell construction and applied current profiles to avoid Li-plating and enable fast charging in BEVs.

Ongoing work focuses on extending this modeling effort to predict the effects of dendrite formation on impedance growth and loss of active material. Furthermore, teardown and post-mortem analysis will be utilized to prove the occurrence of plating and stripping.

Author Contributions: Conceptualization: P.B.R., P.R., J.H.K., M.C.; Methodology: P.B.R., P.R.; Model Development and Validation: P.B.R., M.W., M.C.; Investigation: P.B.R., M.W., P.R., J.H.K., M.C., C.B., J.D.; Resources, C.B., J.D., H.P.; Writing—Original Draft Preparation: P.B.R., M.C.; Writing—Review and Editing: P.B.R., M.W., P.R., J.H.K., M.C., C.B., J.D.; Supervision: C.B., J.D., H.P.; Project Administration: P.R., M.C., J.H.K. All authors have read and agreed to the published version of the manuscript.

Funding: The research activity that led to this work was funded by Ford Motor Company.

Data Availability Statement: The data presented in this study are available on request from the corresponding author. The data are not publicly available due to confidentiality.

Conflicts of Interest: The authors declare no conflict of interest.

References

- Arora, P. Mathematical Modeling of the Lithium Deposition Overcharge Reaction in Lithium-Ion Batteries Using Carbon-Based Negative Electrodes. *J. Electrochem. Soc.* **1999**, *146*, 3543. [[CrossRef](#)]
- Smart, M.C.; Ratnakumar, B.V. Effects of Electrolyte Composition on Lithium Plating in Lithium-Ion Cells. *J. Electrochem. Soc.* **2011**, *158*, A379. [[CrossRef](#)]

3. Fan, J.; Tan, S. Studies on Charging Lithium-Ion Cells at Low Temperatures. *J. Electrochem. Soc.* **2006**, *153*, A1081. [[CrossRef](#)]
4. Jansen, A.N.; Dees, D.W.; Abraham, D.P.; Amine, K.; Henriksen, G.L. Low-temperature study of lithium-ion cells using a LiySn micro-reference electrode. *J. Power Sources* **2007**, *174*, 373–379. [[CrossRef](#)]
5. Huang, C.K.; Sakamoto, J.S.; Wolfenstine, J.; Surampudi, S. The Limits of Low-Temperature Performance of Li-Ion Cells. *J. Electrochem. Soc.* **2000**, *147*, 2893. [[CrossRef](#)]
6. Janakiraman, U.; Garrick, T.R.; Fortier, M.E. Lithium Plating Detection Methods in Lithium-ion Batteries. In *Electrochemical Society Meeting Abstracts Prime2020*; The Electrochemical Society, Inc.: Pennington, NJ, USA, 2020; p. 47.
7. Zier, M.; Scheiba, F.; Oswald, S.; Thomas, J.; Goers, D.; Scherer, T.; Klose, M.; Ehrenberg, H.; Eckert, J. Lithium dendrite and solid electrolyte interphase investigation using OsO₄. *J. Power Sources* **2014**, *266*, 198–207. [[CrossRef](#)]
8. Lu, W.; López, C.M.; Liu, N.; Vaughey, J.T.; Jansen, A.; Dennis W.D. Overcharge Effect on Morphology and Structure of Carbon Electrodes for Lithium-Ion Batteries. *J. Electrochem. Soc.* **2012**, *159*, A566–A570. [[CrossRef](#)]
9. Lin, H.p.; Chua, D.; Salomon, M.; Shiao, H.C.; Hendrickson, M.; Plichta, E.; Slane, S. Low-Temperature Behavior of Li-Ion Cells. *Electrochem.-Solid-State Lett.* **2001**, *4*, A71. [[CrossRef](#)]
10. Subramanian, V.R.; Diwakar, V.D.; Tapriyal, D. Efficient Macro-Micro Scale Coupled Modeling of Batteries. *J. Electrochem. Soc.* **2005**, *152*, A2002–A2008. [[CrossRef](#)]
11. Whittingham, M.S. History, Evolution, and Future Status of Energy Storage. *Proc. IEEE* **2012**, *100*, 1518–1534. [[CrossRef](#)]
12. Rahn, C.D.; Wang, C.Y. *Battery Systems Engineering*; John Wiley & Sons: Hoboken, NJ, USA, 2013.
13. Lin, N.; Röder, F.; Kreuer, U. Multiphysics Modeling for Detailed Analysis of Multi-Layer Lithium-Ion Pouch Cells. *Energies* **2018**, *11*, 2998. [[CrossRef](#)]
14. Smith, K. *Micro/Macro-Scale Modeling for Battery Fast Charge Applications*; National Renewable Energy Lab. (NREL): Golden, CO, USA, 2018; p. 28.
15. Zhao, X.; Yin, Y.; Hu, Y.; Choe, S.Y. Electrochemical-thermal modeling of lithium plating/stripping of Li(Ni 0.6 Mn 0.2 Co 0.2) O₂/Carbon lithium-ion batteries at subzero ambient temperatures. *J. Power Sources* **2019**, *418*, 61–73. [[CrossRef](#)]
16. Yang, X.G.; Leng, Y.; Zhang, G.; Ge, S.; Wang, C.Y. Modeling of lithium plating induced aging of lithium-ion batteries: Transition from linear to nonlinear aging. *J. Power Sources* **2017**, *360*, 28–40. [[CrossRef](#)]
17. Zhang, Z.; Jin, Z.; Wyatt, P. Electrochemical Modeling of Lithium Plating of Lithium Ion Battery for Hybrid Application. *Sae. Int. J. Altern. Powertrains* **2017**, *6*. [[CrossRef](#)]
18. von Lüders, C.; Keil, J.; Webersberger, M.; Jossen, A. Modeling of lithium plating and lithium stripping in lithium-ion batteries. *J. Power Sources* **2019**, *414*, 41–47. [[CrossRef](#)]
19. Brodsky, P.; Canova, M.; Kim, J.H.; Ramesh, P.; Bae, C.; Deng, J.; Park, H. *Calibration of Electrochemical Models for Li-Ion Battery Cells Using Three-Electrode Testing*; SAE Technical Paper: Warrendale, PA, USA, 2020; p. 14. [[CrossRef](#)]
20. Petzl, M.; Danzer, M.A. Nondestructive detection, characterization, and quantification of lithium plating in commercial lithium-ion batteries. *J. Power Sources* **2014**, *254*, 80–87. [[CrossRef](#)]
21. Uhlmann, C.; Illig, J.; Ender, M.; Schuster, R.; Ivers-Tiffée, E. In situ detection of lithium metal plating on graphite in experimental cells. *J. Power Sources* **2015**, *279*, 428–438. [[CrossRef](#)]
22. Schindler, S.; Bauer, M.; Petzl, M.; Danzer, M.A. Voltage relaxation and impedance spectroscopy as in-operando methods for the detection of lithium plating on graphitic anodes in commercial lithium-ion cells. *J. Power Sources* **2016**, *304*, 170–180. [[CrossRef](#)]
23. Yang, X.G.; Ge, S.; Liu, T.; Leng, Y.; Wang, C.Y. A look into the voltage plateau signal for detection and quantification of lithium plating in lithium-ion cells. *J. Power Sources* **2018**, *395*, 251–261. [[CrossRef](#)]
24. Bugga, R.V.; Smart, M.C. Lithium Plating Behavior in Lithium-Ion Cells. *Ecs. Trans.* **2010**, *25*, 241. . [[CrossRef](#)]
25. Bauer, M.; Rieger, B.; Schindler, S.; Keil, P.; Wachtler, M.; Danzer, M.A.; Jossen, A. Multi-phase formation induced by kinetic limitations in graphite-based lithium-ion cells: Analyzing the effects on dilation and voltage response. *J. Energy Storage* **2017**, *10*, 1–10. [[CrossRef](#)]
26. von Lüders, C.; Zinth, V.; Erhard, S.V.; Osswald, P.J.; Hofmann, M.; Gilles, R.; Jossen, A. Lithium plating in lithium-ion batteries investigated by voltage relaxation and in situ neutron diffraction. *J. Power Sources* **2017**, *342*, 17–23. [[CrossRef](#)]
27. Waldmann, T.; Wohlfahrt-Mehrens, M. Effects of rest time after Li plating on safety behavior—ARC tests with commercial high-energy 18650 Li-ion cells. *Electrochim. Acta* **2017**, *230*, 454–460. [[CrossRef](#)]
28. Ren, D.; Smith, K.; Guo, D.; Han, X.; Feng, X.; Lu, L.; Ouyang, M.; Li, J. Investigation of Lithium Plating-Stripping Process in Li-Ion Batteries at Low Temperature Using an Electrochemical Model. *J. Electrochem. Soc.* **2018**, *165*, A2167–A2178. [[CrossRef](#)]
29. Yang, X.; Miller, T. *Fast Charging Lithium-Ion Batteries*; SAE Technical Paper: Warrendale, PA, USA, 2017; p. 12. [[CrossRef](#)]
30. Zinth, V.; von Lüders, C.; Hofmann, M.; Hattendorff, J.; Buchberger, I.; Erhard, S.; Rebelo-Kornmeier, J.; Jossen, A.; Gilles, R. Lithium plating in lithium-ion batteries at sub-ambient temperatures investigated by in situ neutron diffraction. *J. Power Sources* **2014**, *271*, 152–159. [[CrossRef](#)]
31. Hein, S.; Danner, T.; Latz, A. An Electrochemical Model of Lithium Plating and Stripping in Lithium Ion Batteries. *Acs Appl. Energy Mater.* **2020**, *3*, 8519–8531. [[CrossRef](#)]
32. Konz, Z.M.; McShane, E.J.; McCloskey, B.D. Detecting the Onset of Lithium Plating and Monitoring Fast Charging Performance with Voltage Relaxation. *Acs Energy Lett.* **2020**, *5*, 1750–1757. [[CrossRef](#)]

33. Konz, Z.M.; McShane, E.J.; McCloskey, B.D. *Voltage Relaxation to Detect the Onset of Lithium Plating on Graphite for Fast Charging*; p. 19. Available online: <https://chemrxiv.org/engage/chemrxiv/article-details/60c74a07bdbb898b2ea392d6> (accessed on 8 May 2023).
34. Carter, R.; Klein, E.J.; Kingston, T.A.; Love, C.T. Detection of Lithium Plating During Thermally Transient Charging of Li-Ion Batteries. *Front. Energy Res.* **2019**, *7*, 144. [[CrossRef](#)]
35. Doyle, M. Modeling of Galvanostatic Charge and Discharge of the Lithium/Polymer/Insertion Cell. *J. Electrochem. Soc.* **1993**, *140*, 1526. [[CrossRef](#)]
36. Sulzer, V.; Marquis, S.G.; Timms, R.; Robinson, M.; Chapman, S.J. Python Battery Mathematical Modelling (PyBaMM). *J. Open Res. Softw.* **2021**, *9*. [[CrossRef](#)]

Disclaimer/Publisher's Note: The statements, opinions and data contained in all publications are solely those of the individual author(s) and contributor(s) and not of MDPI and/or the editor(s). MDPI and/or the editor(s) disclaim responsibility for any injury to people or property resulting from any ideas, methods, instructions or products referred to in the content.